ANALYSIS OF MAGNETIC RAYLEIGH-TAYLOR INSTABILITY AND ITS EFFECT ON ANGULAR MOMENTUM TRANSPORT IN A BLACK HOLE ACCRETION DISK

By

MAX HANRAHAN

A senior thesis submitted in partial fulfillment of
the requirements for the Senior Project

HAMILTON COLLEGE
Physics

MAY 2022

ACKNOWLEDGMENT

I would like to thank Hamilton College Professors Viva Horowitz, Brian Collett, Clark Bowman, and Tural Sadigov for helping me sanity-check and interpret a few surprising results. I would also like to thank my parents, Jack and Kim Hanrahan, for their love and support.

ANALYSIS OF MAGNETIC RAYLEIGH-TAYLOR INSTABILITY AND ITS EFFECT ON ANGULAR MOMENTUM TRANSPORT IN A BLACK HOLE ACCRETION DISK

Abstract

by Max Hanrahan, Bachelor's
Hamilton College
May 2022

Faculty Advisor: Megan Marshall Smith

A strong vertical magnetic field in a black hole accretion disk system can suppress magnetorotational instability (MRI), so the transport of angular momentum within the disk may be driven by other fluid instabilities. We examine the simulation of a magnetically arrested disk (MAD) exhibiting magnetic Rayleigh-Taylor (RT) instability, in which low-density regions of plasma push against high-density regions and cause turbulence. Our analysis of the MAD during one specific RT event is consistent with previous findings that outward angular momentum transport diminishes during one of these events, and that the largest contribution to MAD stress is its turbulent component.

TABLE OF CONTENTS

Chapter One

Introduction

In 1915, Albert Einstein published his general theory of relativity [1]. Shortly afterward, Karl Schwarzschild published a solution to Einstein's field equations, which predicted the existence of spherical objects with a point of infinite density and gravity so strong that not even light could move fast enough to escape its gravitational pull [2]. For decades, experts in the field of general relativity doubted the existence of these objects. However, one such phenomenon was first observed by NASA's Uhuru X-ray Explorer Satellite in 1970, shortly after physicist John Wheeler coined the term "black hole" [3].

Since then, black holes (BHs) have fascinated astronomers, scientists, and the general public. They are often studied by observing their surrounding matter, since a telescope with high enough resolution to observe an isolated BH was not developed until 2019 [4]. Astronomers have observed x-ray emissions due to matter accreting onto a BH, indicating the presence of an accretion disk. These disks form through phenomena such as a tidal disruption event (in which a star comes sufficiently close to a BH and is torn apart by its strong gravity), or the collapse of a binary system (in which the more massive object becomes a BH and envelops the smaller object). Observations of matter accreting onto the BH indicate that the plasma must lose angular momentum as it rotates. Therefore, there must be an instability that causes surrounding matter to lose angular momentum and fall into the BH, increasing its mass and gravitational field.

We examine the simulation of a thin magnetically-arrested disk (MAD) of gas and plasma rotating around a central BH. These disks are characterized by their strong, vertical magnetic field [5]. This magnetic field causes the disk to be susceptible to Rayleigh-Taylor (RT) events, in which low-density regions of fluid push against high-density regions of fluid against the direction of gravitational acceleration [6]. The simulation's original authors predicted that such events would lead to outward angular momentum transport in the disk, thereby causing matter in the disk to lose enough angular momentum as to fall in to the central BH and increase its mass [7]. However, later analysis by Marshall et al. confirmed that the formation of the largest RT event in this simulation hindered accretion, rather than facilitating it [8]. In this paper, I examine the effectiveness of RT instability as a possible cause of angular momentum transport in a thin MAD rotating around a BH.

Following this introduction is a discussion of the necessary theoretical framework for BH physics, and a description of the events we study. Chapter Three outlines the specifics of our simulation. In Chapter Four, I present an analysis of our studied event. In Chapter Five, I state my conclusions.

Chapter Two

Background

2.1 Black Hole Fundamentals

A BH is defined by only three unique properties: mass, charge, and spin (this is known as the "no-hair theorem" of General Relativity) [9]. By mass, BHs belong to one of three categories: "stellar mass" (on the order of 1-10$M_\odot$, where $M_\odot$ is one solar mass), "intermediate mass" (on the order of $M = 1000M_\odot$), and "supermassive" (on the order of $M = 10^5 M_\odot$). Our BH is supermassive, represented by a dimensionless quantity of $M = 1$ in the simulation code.

The spin parameter, referred to as a in the Kerr metric in the following section, is a constant parameter describing an object's rotation that ranges from -1 to 1 in dimensionless form. It is defined as $a \equiv J/Mc^2$, where M is the mass of the rotating body, J is its angular momentum, and c is the speed of light. Negative a represents retrograde motion, (i.e., the BH and the accretion disk are spinning in opposite directions), while positive a/M represents prograde motion (where the BH and its disk are spinning in the same direction). Our simulation has a fixed at $+0.5$.

Our BH has no charge. The general metric for a spinning, charged, and spherically symmetric object is called the Kerr-Newman metric, and includes a parameter Q for the rotating object's charge [10]. The Kerr-Newman metric reduces to the Kerr metric in the $Q = 0$ case (which is the charge of the BH we are studying). These three properties (positive

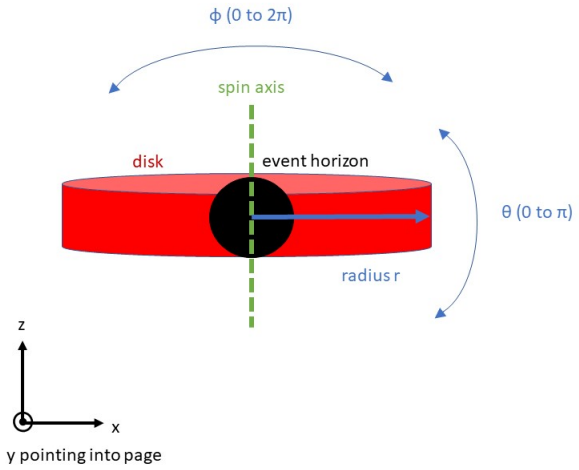

Figure 2.1 Simple schematic diagram of the simulated system. The z-axis (represented by a green dashed line) is aligned with the spin axis for the BH and the disk, and perpendicular to the disk. The disk is fixed at $\theta = 0$, where θ is the azimuthal angle and ϕ is the polar angle. The radial coordinate r is represented by the blue arrow in the $z = 0$ plane.

spin, zero charge, and large mass) make our BH comparable to other spinning, supermassive BHs (SMBHs) such as Sagittarius A* (Sgr A*) and Messier 87 (M87). Figure 2.1 is a schematic of the BH in a Cartesian and spherical coordinate system.

2.2 General Relativity

Einstein's general theory of relativity is a useful theory in determining the curvature of spacetime and movement of matter in the presence of a strong gravitational field. Famously, the physicist John Wheeler summarized the physical meaning of Einstein's field equations as "spacetime tells matter how to move, matter tells spacetime how to curve" [11]. The first solutions to these equations were found by Karl Schwarzschild. Intending to describe the dynamics of a spherically-symmetric object in the absence of charge or angular momentum, Schwarzschild formulated a metric for describing the geometry of spacetime in a "polar-like" coordinate system. This metric has since proven useful for describing the gravitational

effects of large celestial bodies undergoing negligible rotation. The Schwarzschild metric in relativistic units (such that c = 1) is

$$ds^2 = -\left(1 - \frac{2GM}{r}\right) dt^2 + \left(1 - \frac{2GM}{r}\right)^{-1} dr^2 + r^2(d\theta^2 + \sin^2\theta d\phi^2), \tag{2.1}$$

where M is the object's mass and r is the circumferential radial coordinate. In 1963, Roy Kerr formulated a more general metric that accounted for uncharged rotating bodies, such as the BH we are studying. The Kerr metric in relativistic units is

$$ds^2 = -(1-\frac{2Mr}{\rho^2})dt^2 - \frac{4Mar\sin^2(\theta)}{\rho^2}d\phi dt + \frac{\rho^2}{\Delta}dr^2 + \rho^2 d\theta^2 + \left(r^2 + a^2 + \frac{2Mra^2\sin^2(\theta)}{\rho^2}\right)\sin^2(\theta)d\phi^2, \tag{2.2}$$

where $a = J/M$ is the spin parameter, $\rho^2 = r^2 + a^2\cos^2(\theta)$, and $\Delta = r^2 - 2Mr + a^2$. [12] This is the metric that our simulated BH system obeys.

2.3 Accretion Disk Theory

Accretion disks are circular disks of rotating matter that form around a central gravitational body. In BH systems, accretion disks are composed of gas and plasma. Using conservation of angular momentum, early theoretical models predicted that this plasma should remain in orbit forever. However, observations of BH accretion disks have indicated that matter in the accretion disk tends to fall in to the black hole, producing high-energy "jets" of x-ray and gamma-ray bursts. Since these jets require a significant amount of energy to produce, astronomers have determined that matter must fall into the BH, rather than remain in orbit around the accretion disk. There must therefore exist some type of instability that causes angular momentum to dissipate within the accretion disk.

2.4 Magnetorotational Instability (MRI)

In one model of BH accretion known as Standard and Normal Evolution (SANE), there exists a weak and turbulent magnetic field that acts as a restoring force [13]. This means that particles attached by a magnetic field line in the plasma disk may initially be close together, but those closer to the center will have a higher tangential velocity by conservation of angular momentum. This causes the particles to drift apart as they orbit the BH, whereupon the distance between them increases the magnitude of a spring-like magnetic restoring force. This causes the inner particle (which orbits faster) to transfer its angular momentum to the outer particle, which then causes the particles to drift apart even more. This then increases the restoring force between the particles, and the process repeats. This model of the "restoring" force, ironically, is what leads to the instability of the disk. Figure 2.2

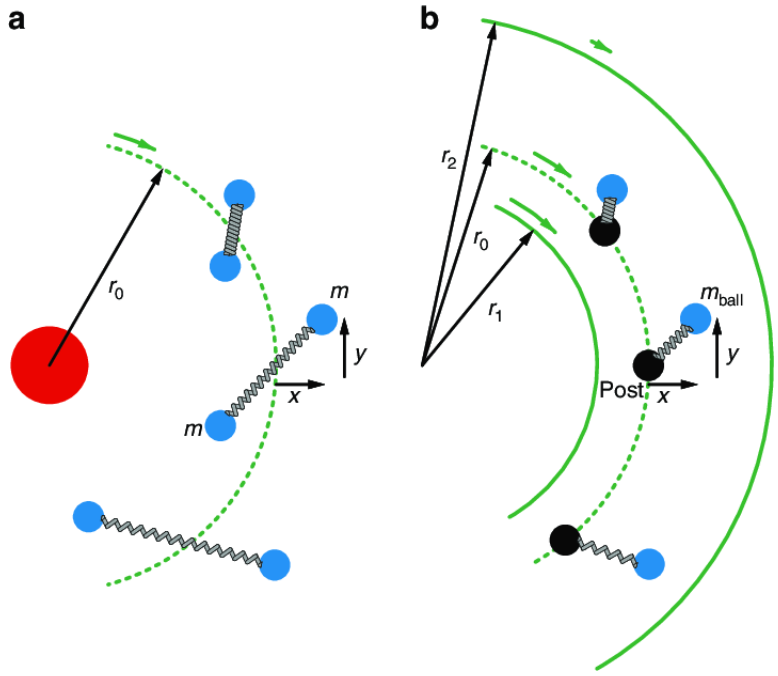

Figure 2.2 For a spinning disk in a weak, purely vertical magnetic field, it is a useful analogy to imagine the magnetic force between particles as springs.

[14]

(below) is an illustration of this process.

However, this model of instability is suppressed in accretion disks with strong magnetic fields, because the restoring force is too high to create the feedback loop described above [13]. Models of such disks must therefore incorporate another type of instability which will lead to outward angular momentum transport, and thus accretion.

2.5 Rayleigh-Taylor Instability

One such instability is RT Instability, which occurs when a high-density fluid pushes against a low-density fluid, as depicted in Figure 2.3 below. A specific type of this instability occurs

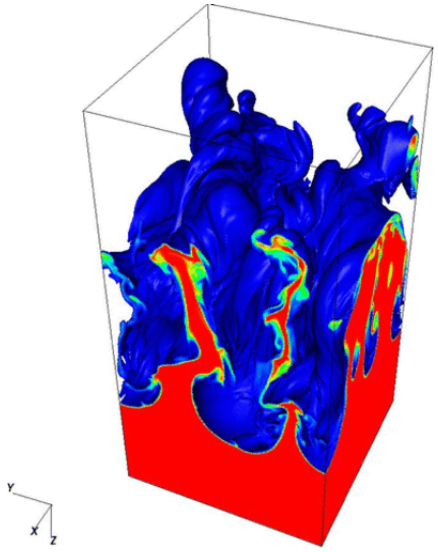

Figure 2.3 A magnetic Rayleigh-Taylor (RT) event, where a low-density (blue, top) fluid pushes against a high-density (red, bottom) fluid and creates finger-like instability. Note that in this diagram, the gravitational field points up.

[6]

in plasma in the presence of a magnetic field, called magnetic RT instability, [6] wherein the heavier fluid is "on top of" the lighter fluid with respect to gravity, and the magnetic field is present between the two of them. The pressure inside the gas causes buildup of flux on the event horizon, which in turn causes the magnetic field outside of the BH to become so strong that it disrupts the axisymmetric accretion flow [15]. This results in large amounts

of flux getting pushed off the BH and onto the disk, as well as the emergence of low density "bubbles" and fluctuations of stress (internal force per unit area) throughout the disk. These bubbles, traveling upward in the disk, are surrounded by downward-moving streams of high-density plasma, and as such, a low-density fluid pushes against a high-density fluid. In our simulation, these "RT events" can be found flaring up during significant decreases in the magnetic field across the BH event horizon. As such, RT events are potential candidates for causing the transport of angular momentum within the disk. Figure 2.4 (below) is a screenshot of one such event in our simulation.

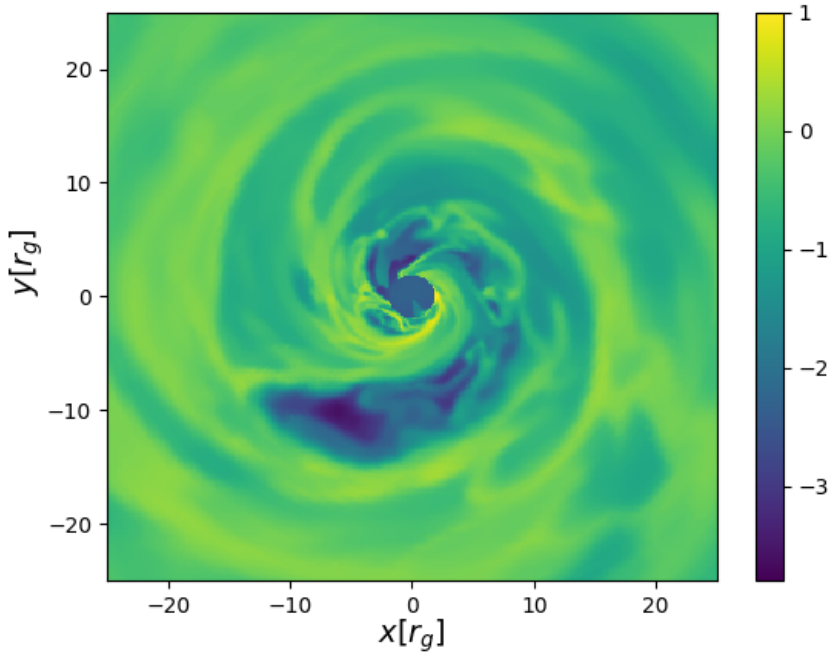

Figure 2.4 A base-10 logarithmic density render of an RT event in the $z = 0$ plane. Note the presence of the low-density "bubble" region.

2.6 Effective Viscosity

The ultimate goal of our research is to examine what factors contribute to the disk's angular dynamics. As such, we require a quantitative way of determining the outward transport of angular momentum. As first suggested by Shakura and Sunyaev, we characterize this

angular momentum transport by measuring the disk's effective viscosity v [16]. This quantity is proportional to a dimensionless quantity α through the following relation:

$$v = \alpha c_s H, \tag{2.3}$$

where c_s is the speed of sound within the disk, and H is the disk's half-height. In most cases, c_s and H will be constant, so we investigate angular momentum transport using the dimensionless parameter α. The parameter α is proportional to the $r-\phi$ component of the Maxwell stress energy tensor, and defined as

$$\alpha \equiv -\frac{b_r b_\phi}{\langle P_{\rm b} + P_{\rm gas} \rangle}, \tag{2.4}$$

where b_r and b_ϕ are, respectively, the r and ϕ components of the magnetic four-velocity in the frame of the rotating fluid, and the denominator is the total pressure in the disk. This is the sum of disk gas pressure $P_{\rm gas} = (\Gamma - 1)U_g$ and magnetic pressure $P_{\rm b} = \frac{1}{2}|B|^2$ where U_g is the potential energy of the gas, Γ is the adiabatic index, and $|B|$ is the magnitude of the magnetic field. [8].

To determine factors driving the transport of angular momentum throughout the disk, we measure α as a time-series during RT events and compare to other measurable quantities.

2.7 Previous Findings

Marshall et al. [8] analyzed the largest RT event produced in the simulation from Avara et al. [7], and found that the stress in the disk was lowered by the emergence of the bubble, ultimately hindering accretion. Several previous student theses have continued examining the relationship between RT events and accretion in the disk. They have done so by studying a specific period in the simulation in which low-density bubbles form, and analyzing the magnetic stress in both the low-density bubble region and surrounding disk (where magnetic stress is defined to be the $r-\phi$ component of the Electromagnetic Stress Tensor, integrated

throughout the region in question). They observed that the greatest contribution to this stress was its turbulent component, in both the low-density region and the surrounding accretion disk [17] [18] [19]. These results are consistent with Marshall's findings. In particular, Sirabian [17] noticed a strong, positive, and linear correlation between α and the magnetic flux across the BH event horizon. However, she found no evidence of a significant time delay between these two quantities, and concluded that there may be a third quantity influencing the dynamics of both α and this event-horizon magnetic flux.

Chapter Three

Our Simulation

3.1 Assumptions

Our simulation, originally coded by Avara et al. [7], is a thin magnetically arrested disk (MAD). An accretion disk with half-height H and radius r is categorized as "thin" if H/r is on the order of 0.1 radians, and "thick" otherwise. This condition lets us more easily analyze the low-density RT events due to the absence of excessive matter [8]. Our modeled plasma consists of only electrons, because their low mass allows them to achieve much higher speeds. As such, they are responsible for most of the dynamics we are interested in studying. Further, including only electrons in the simulation has the added effect of being more computationally efficient.

In addition, our model assumes ideal magnetohydrodynamics (MHD): the study of magnetic interactions in the context of fluid dynamics. The "ideal" condition is this: in an ideal fluid, the magnetic field may attach itself to a patch of moving matter, and become "frozen in" with the motion of the fluid (for this reason, it is often referred to as the "frozen in" condition of MHD) [20]. The simulation code also contains a cooling function to keep the disk thin and at a constant angle ($\theta = 0.1$) during the simulation.

Our model is fully general relativistic and contains no Newtonian approximations, and is thus considered a general relativistic magnetohydrodynamic (GRMHD) simulation of the

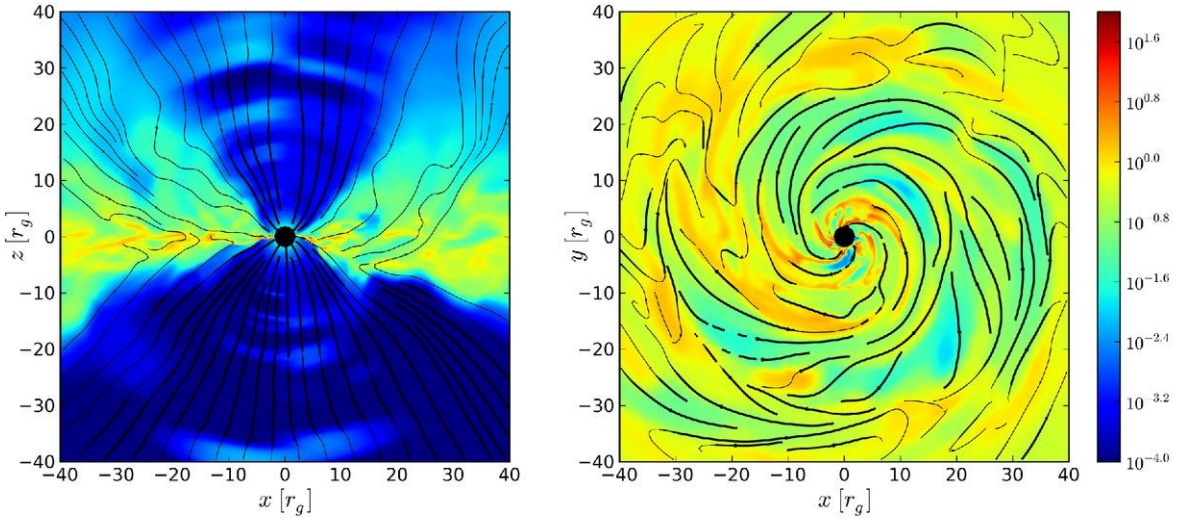

Figure 3.1 The xz cross-section (left) and xy cross-section (right) of a density plot of the accretion disk at an arbitrary timestep. The z-axis is aligned with the spin axis of the BH and accretion disk.

[7]

accretion disk. It is also fully three-dimensional and global, as the first authors of the simulation were initially interested in examining outflows. This is in contrast to other models that may simulate a wedge of the disk for computational efficiency, rather than the entire accretion disk. Figure 3.1 (above) illustrates a "side view" and "top view" of the density at a point in time.

3.2 Our Data

For the sake of scalability, we leave physical distance in terms of gravitational radius r_g, defined to be half the Schwarzschild radius: $r_g = \frac{1}{2}\left(\frac{2GM}{c^2}\right) = \frac{GM}{c^2}$. We can then use this scalable radius to construct a dimensionless unit of time, r_g/c. Our simulation evolves over the course of 69,268 r_g/c. The real-time evolution of a comparable, observable BH depends on its mass, as described by table 3.1 below. For instance, a BH as large as M87 will experience $69,268 r_g/c$ over the course of decades, whereas a relatively smaller SMBH such as Sgr A* could experience this evolution over the course of mere days.

Characteristic	Sagittarius **A***	**M87***
Mass	$4.154 \pm 0.014 \times 10^6 M_\odot$	$6.5 \pm 0.7 \times 10^9\ M_\odot$
Gravitational Radii (r_g)	$6.13 \pm 0.02 \times 10^9$ m	$9.6 \pm 1.0 \times 10^{12}$ m
Schwarzschild Radius	$1.226 \pm 0.004 \times 10^{10}$ m	$1.9 \pm 0.2 \times 10^{13}$ m
Size of MAD Region	$2.452 \pm 0.008 \times 10^{11}$ m	$3.8 \pm 0.4 \pm \times 10^{14}$ m
Duration of r_g/c	20.46 ± 0.07 s	8.9 ± 1.0 hrs
Duration of Simulation	16.40 ± 0.06 days	70 ± 7 years

Table 3.1 Simulation properties when applied to Sagittarius A* and M87*

We analyze the evolution of the accretion disk by measuring its mass density and magnetic field lines. Our magnetic field is initially strong, uniform, and highly vertical, which ensures the creation of a MAD region in the disk. Figure 3.2 (below) is a plot of the initial distribution of plasma and magnetic field strength surrounding the BH.

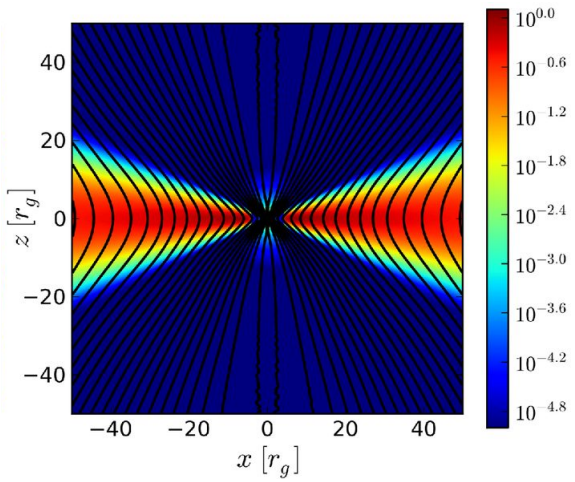

Figure 3.2 The xz cross-section of the simulated system at $t = 0$. The colormap indicates the base-10 logarithmic rest-mass density and the black lines are magnetic equipotentials.

Chapter Four

Analysis and Results

4.1 Stress Analysis

I chose a previously unexamined RT event to analyze, with the intent of investigating the relationship between RT instability and angular momentum transport. This particular event featured several low-density sections of fluid that stayed close to the BH, which distinguishes this event from other previously-studied events. This is advantageous in isolating the stress in the RT bubble from stress in the remainder of the disk, as will be discussed later in this section. A plot of the stress parameter α with respect to time reveals that total stress decreases as the RT bubble flares up, corresponding to a decrease in outward angular momentum transport. This is depicted in Figure 4.1 below.

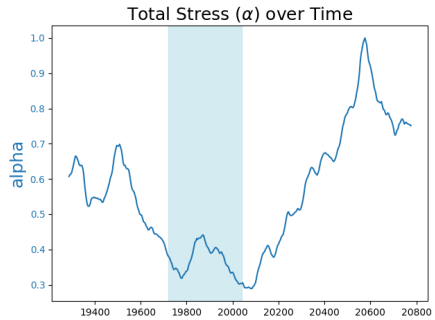

Figure 4.1 A plot of our stress parameter α over time, which we use to characterize the transport of outward angular momentum throughout the disk. The RT event flares up in the highlighted region, during a significantly sharp decrease in the total stress.

This result is consistent with previous findings from similar RT events in this simulation [8] [17] [18] [19].

Further, we are able to analyze stress by breaking up α into components and quantitatively determining which term is the dominant contributor. To separate the effect of the mean field from the turbulent field, b_r and b_ϕ are divided into $\langle b_r \rangle + \delta b_r$ and $\langle b_\phi \rangle + \delta b_\phi$ respectively. When substituted into Equation 2.4, this gives:

$$\alpha \equiv -\frac{b_r b_\phi}{P_{\text{Total}}} = -\frac{1}{P_{\text{Total}}} \left(\langle b_r \rangle_t + \delta b_r\right) \left(\langle b_\phi \rangle_t + \delta b_\phi\right)$$
$$= -\frac{1}{P_{\text{Total}}} \Big(\langle b_r \rangle_t \langle b_\phi \rangle_t + \langle b_r \rangle_t \delta b_\phi + \langle b_\phi \rangle_t \delta b_r + \delta b_r \delta b_\phi \Big). \quad (4.1)$$

The first term is α's mean component, the last term is its purely turbulent component, and the middle two are cross terms. This decomposition allows us to compare α's four components and compare their evolution throughout the duration of the event. Consistent with previous findings [8] [17] [18] [19], we observe that the dominant stress component is the turbulent term, and the two cross terms are near-zero and negative for the majority of the RT event. Figure 4.2 is a plot of our analysis of stress throughout the entire accretion disk.

However, it is possible to examine the angular momentum transport specifically within the low-density region by "filtering" the data. We do this using inverse plasma beta (β^{-1}):

$$\beta^{-1} \equiv \frac{P_{\text{b}}}{P_{\text{gas}}} \quad (4.2)$$

Using fundamental quantities, we can express β^{-1} like so:

$$\beta^{-1} = \frac{\frac{1}{2}|B|^2}{(\Gamma - 1)U_g}. \quad (4.3)$$

From this relation, we see that β^{-1} is high in regions with low gas pressure and strong magnetic field. Since an RT event is a low-density region formed by the buildup of magnetic

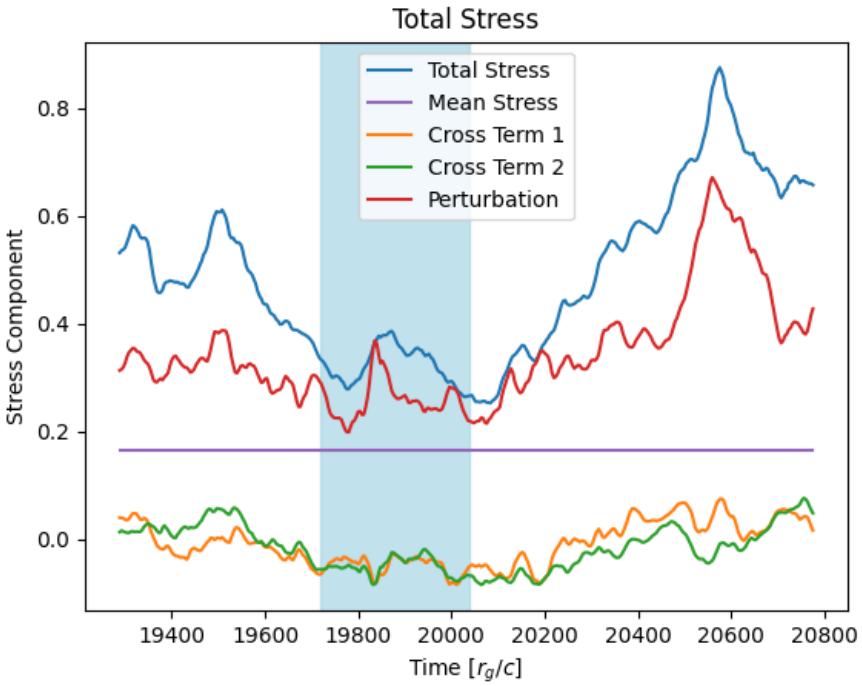

Figure 4.2 The plot of each stress component in Equation 4.1 during the RT event. Below the top "Total Stress" time series is the "Perturbation" (purely turbulent) component. Below this on the plot is the mean contribution to stress (constant with respect to time), and below this are the two cross term contributions, which are centered around zero, and negative for the duration of the simulation. The bubble is at its largest from approximately 19720 r_g/c to 20040 r_g/c, and is indicated by a highlighted region in which we see a sharp decrease in total stress. Following this highlighted region, the total stress recovers over a longer time interval.

flux on the event horizon that then moves out across the disk, the bubble region will have exactly this combination of low pressure (due to low density) and high magnetic field. We can therefore filter the stress data by only examining the stress in the disk corresponding to regions in which β^{-1} is above a certain threshold. This allows us to isolate the stress in the bubble region and examine its four components.

To determine this threshold, we created renders of β^{-1} at the times where the RT event was most prominent, at various thresholds. We then found a value for the smallest possible upper-limit of β^{-1} that would capture the visual features of the bubble region (as shown in Figure 4.3 below), while filtering out the remainder of the disk, including the low-density patches that are not part of the RT event. We then used this threshold to mask the bubble region, and repeated the stress analysis for the bubble region specifically (which we call "bubble stress" in Figure 4.4 below) and the entire disk excluding the bubble region (which we call "disk stress" in Figure 4.5 below).

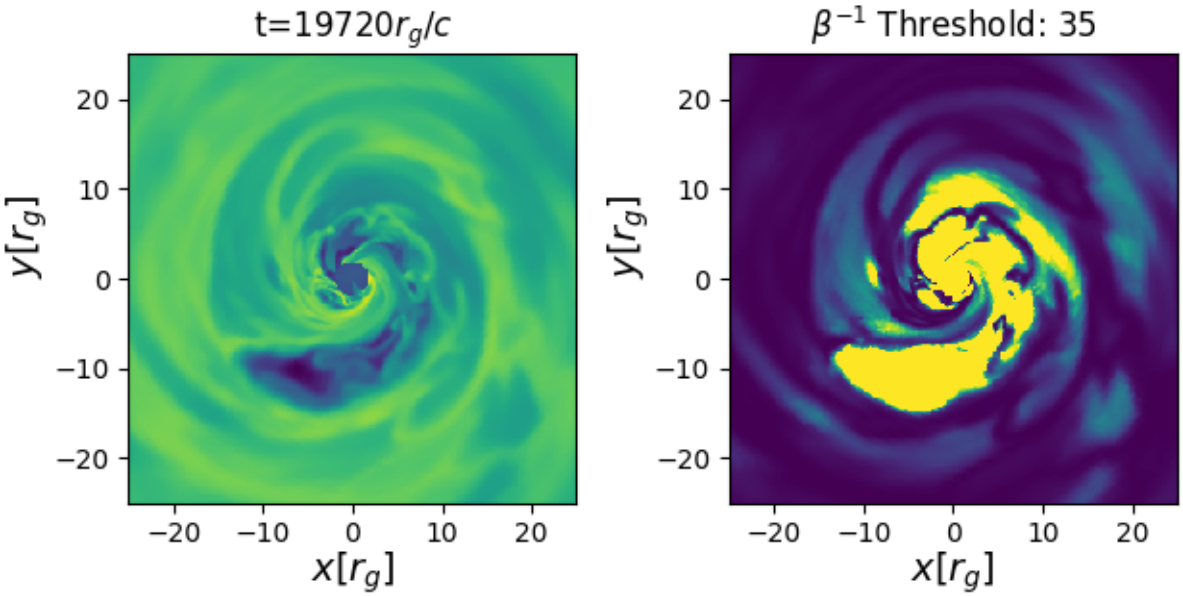

Figure 4.3 A plot of density (left) and inverse β (right). The maximum value of β^{-1} is adjusted until only the features of the bubble and surrounding low-density patches remain in the plot. Once obtained, we can use this β^{-1} threshold to filter stress data, and perform an analysis within the bubble only.

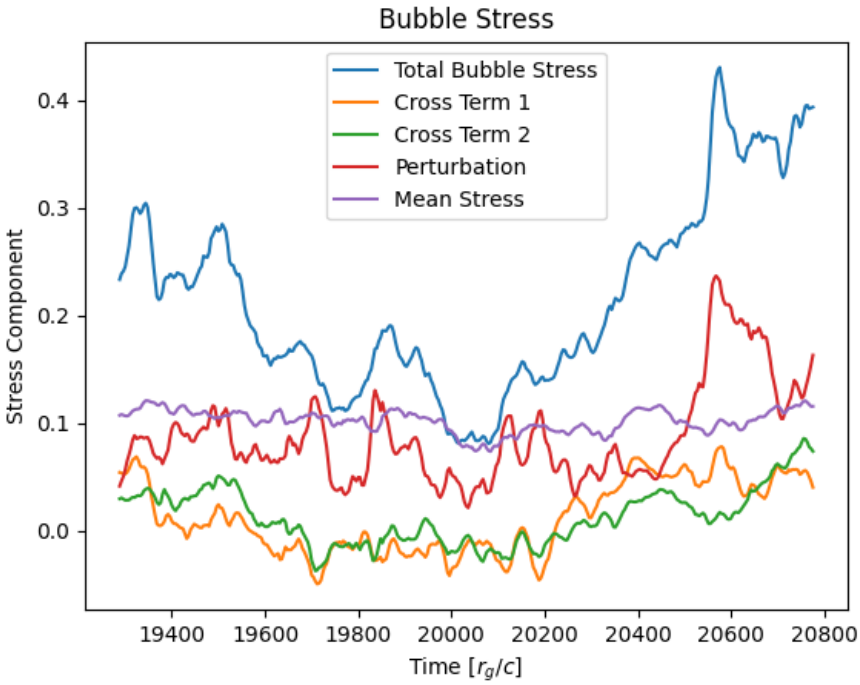

Figure 4.4 A plot of each stress component of Equation 4.1 in the bubble region. We again find that the Perturbation component dominates in this region, and the cross terms are centered around zero.

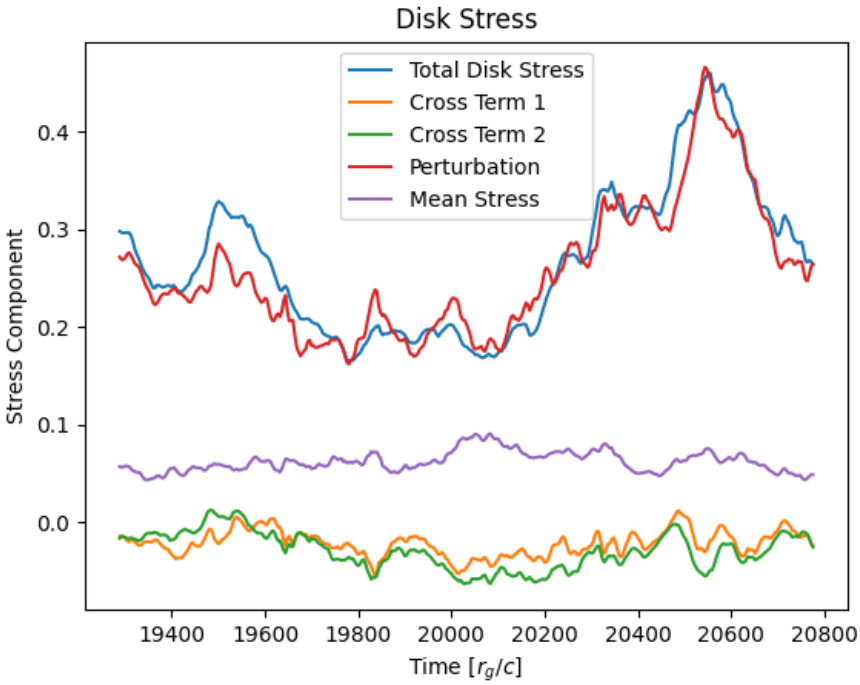

Figure 4.5 A plot of each stress component of Equation 4.1 in the entire plane, excluding the bubble region. As above, we find that the Perturbation component is the dominant contribution, and the cross terms are centered around zero.

4.2 Relationship to Magnetic Field

As described in Chapter 2, RT events are known to occur during a sharp decrease in the event-horizon magnetic flux Υ. Figure 4.6 (below) depicts the time series of total stress

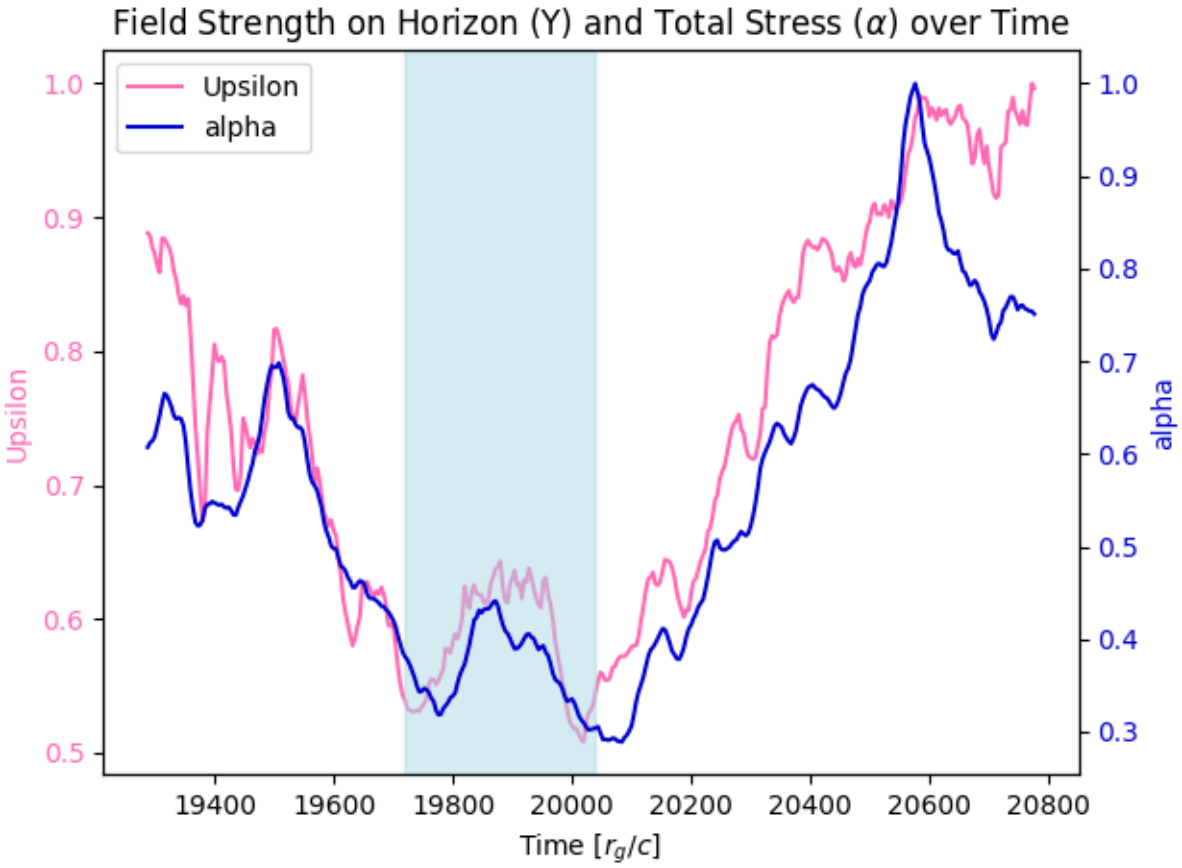

Figure 4.6 A time-series plot of total stress (α) and magnetic flux on the event horizon (Υ), both plotted against time. The highlighted region indicates the RT event, which corresponds to a sharp decrease in both Υ and α. Following this is region is a slow recovery.

α and event-horizon magnetic flux Υ. From this plot, it may appear that there is a time lag between Υ and α, since the two plots share many similar qualitative features. For instance, the magnetic flux appears to significantly and sharply decrease shortly before the sharp and significant decrease observed in total stress, which would suggest that magnetic flux may influence the dynamics of the disk. However, computing the time-dependent cross

correlation of these two functions does not suggest a time delay between α and Υ, even in specific regions of the plot where Υ's apparent lead is more dramatic. Additionally, we can filter for noise by smoothing the data using a Savitzky-Golay filter. Doing so indicates that there is much more agreement between the two time-series, as shown in Figure 4.7 below. This suggests that both α and Υ may be influenced by a lurking variable.

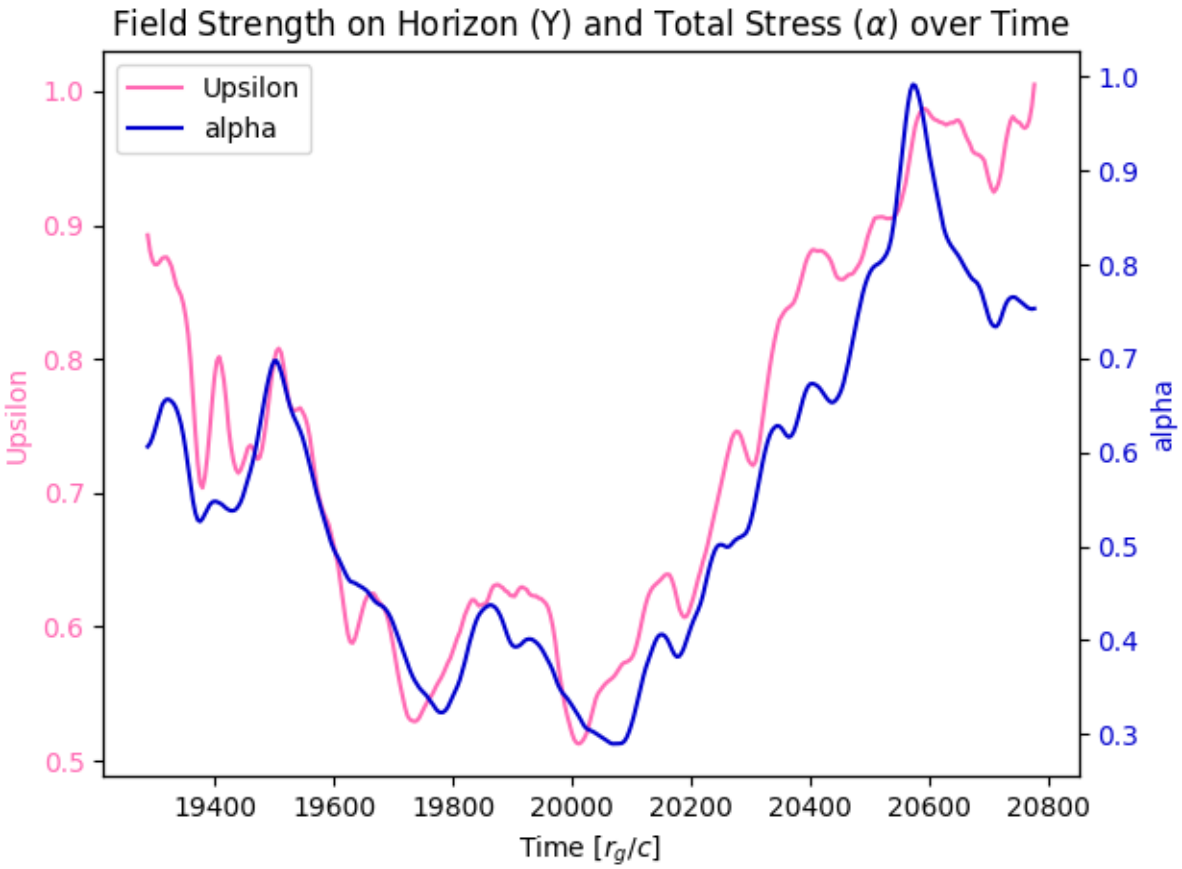

Figure 4.7 A version of Figure 4.6 in which the data are filtered for noise.

4.3 Investigation of Other Possible Driving Factors

4.3.1 Gas Pressure

Our first candidate for a lurking variable was the average gas pressure in an annulus of the disk. We thus broke up the accretion disk into three regions: an "inner annulus" from radius $2.5r_g/c$ (just outside the event horizon) to a radius of $8r_g/c$, outside of which the RT event stayed for the duration of the simulation, a "middle annulus" that contains the entirety of the RT event, and an "outer annulus" that contains only higher-density matter, as shown below in Figure 4.8. Thus, the dynamics of the bubble are contained within the middle annulus, separate from the gas closest to the BH (inner annulus) or the remainder of the disk (outer annulus).

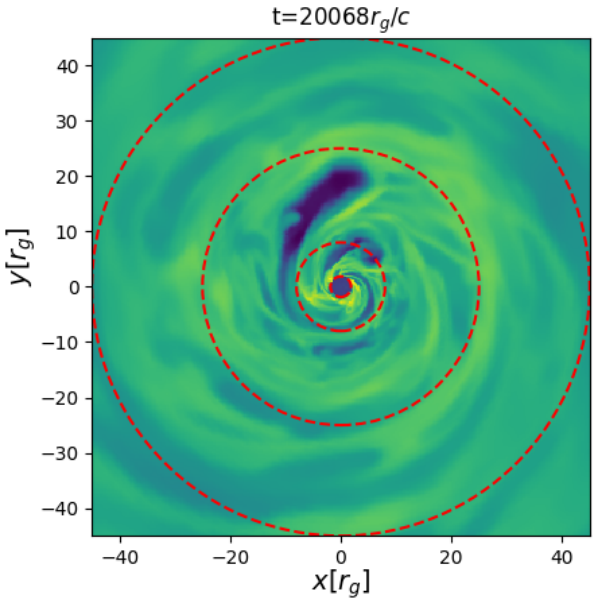

Figure 4.8 A schematic of the three annuli we consider. The first annulus ranges from the innermost circle (encircling the event horizon) to a circle of radius $8r_g$, which osculates the inner portion of the event horizon during most of the simulation's runtime. The next annulus ranges from the circle of radius $8r_g$ to the circle of radius $25r_g$, which contains the entirety of the RT event as it flares up throughout the simulation, as shown in this figure. The outer annulus ranges from $25r_g$ to $45r_g$ and captures the high-density gas outside of the RT event.

We normalize these three quantities such that their maximum value becomes one during the RT event, and plot them with respect to time to reveal that the gas pressure of the inner disk shares many of the same qualitative features as α and Υ. This is shown below in Figure 4.9.

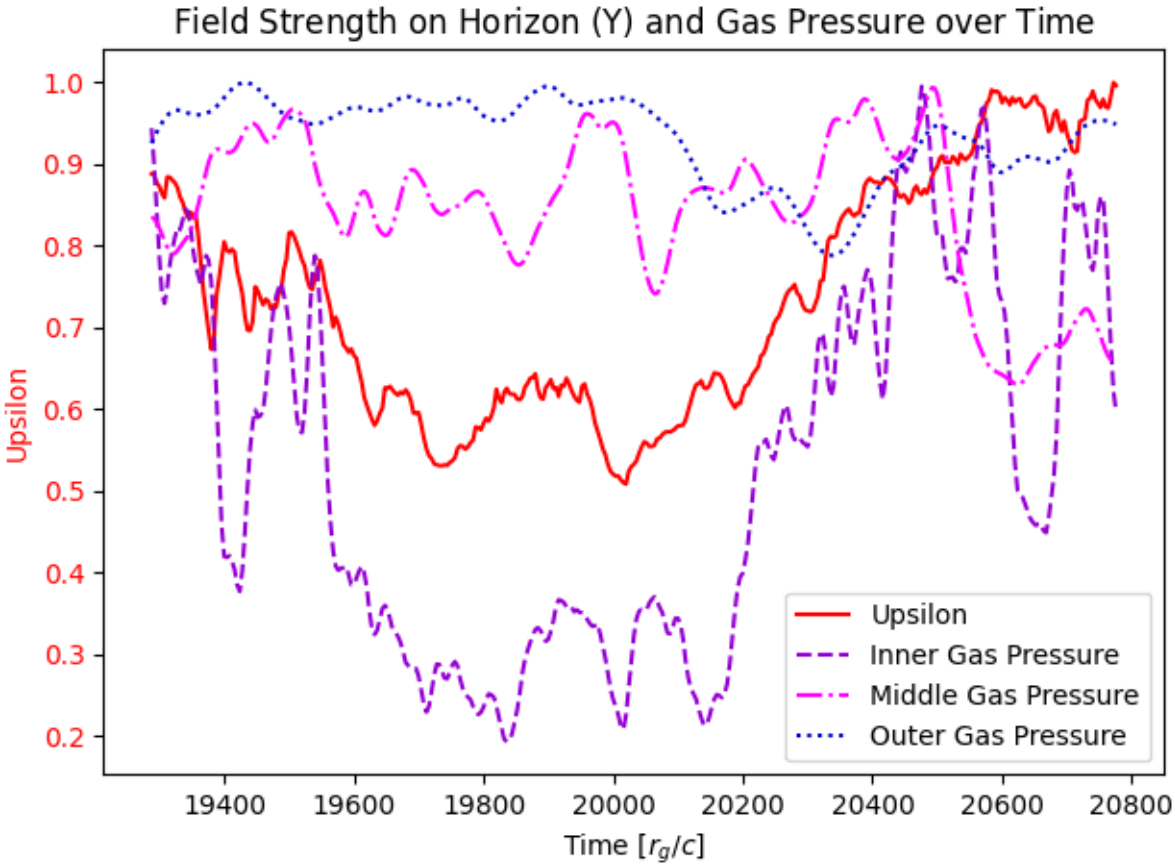

Figure 4.9 Normalized gas pressure plotted as a time series with Υ. Notice how the gas pressure of the inner annulus (violet, dashed line, bottom) bears a resemblance to the graph of event horizon flux (red, solid line). Also included in this plot is the gas pressure in the middle annulus (pink, dot-dashed line) and the gas pressure in the outer annulus (blue, dotted line).

The gas pressure in the outer rings do not bear such a resemblance, and so we disregarded them for the rest of the analysis. However, correlating horizon field strength with this inner-annulus gas pressure reveals that there is no significant time delay, and in fact, the pressure may be trailing Υ, as shown in Figure 4.10.

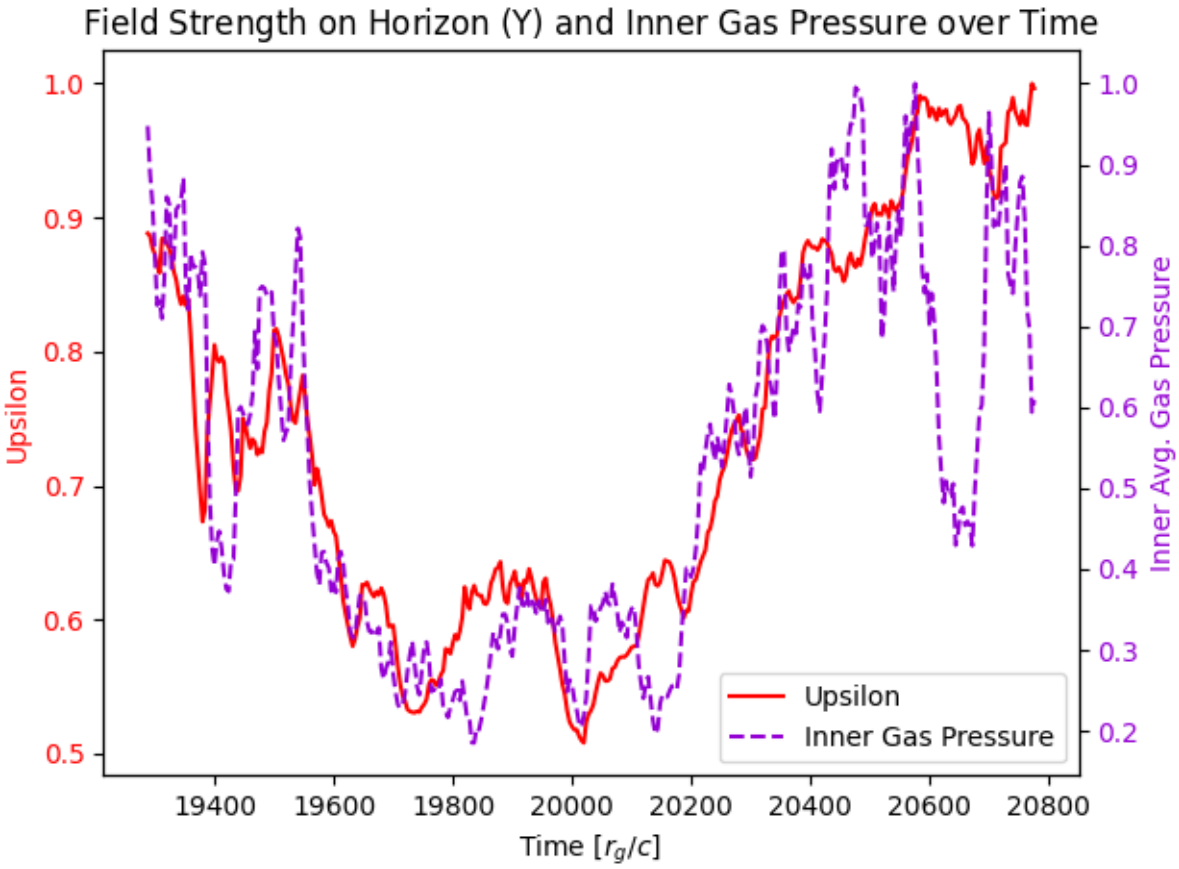

Figure 4.10 A plot of normalized gas pressure of the inner region (dashed, violet) with Υ (solid, red). They share many of the same qualitative features, but by inspection it appears that Υ does not trail the inner average gas pressure.

4.3.2 Average Density

Similarly, we normalized and plotted the average densities in these three regions. Of the time series in these three regions, Υ shares most of its features with the density in the inner annulus, just as we found for gas pressure above.

Just as before, we correlated Υ and inner annulus density and did not find any evidence to suggest a significant time delay between Υ and inner annulus density.

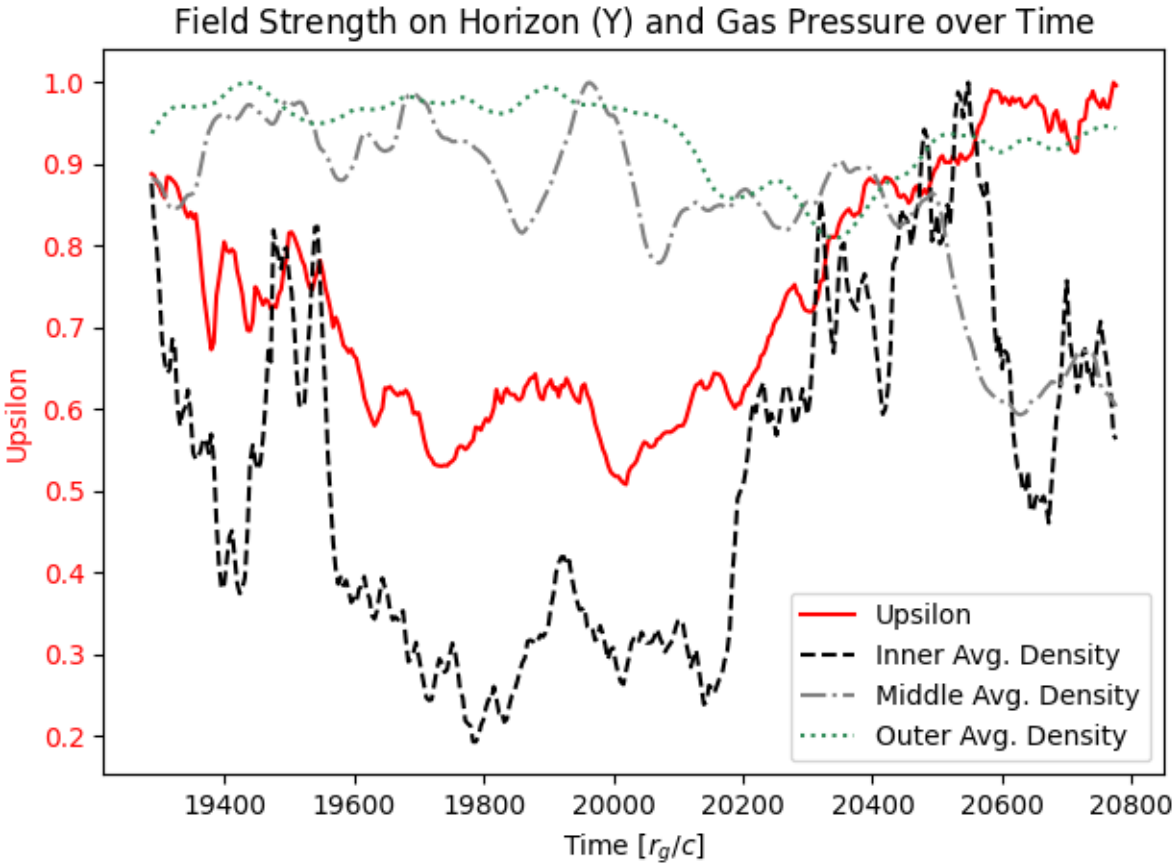

Figure 4.11 A similar graph to Figure 4.9 above, but with average density instead of pressure in the three annuli. Υ is the red solid line, inner average density is the black dashed line, middle average density is the grey dot-dashed line, and outer average density is the green dotted line.

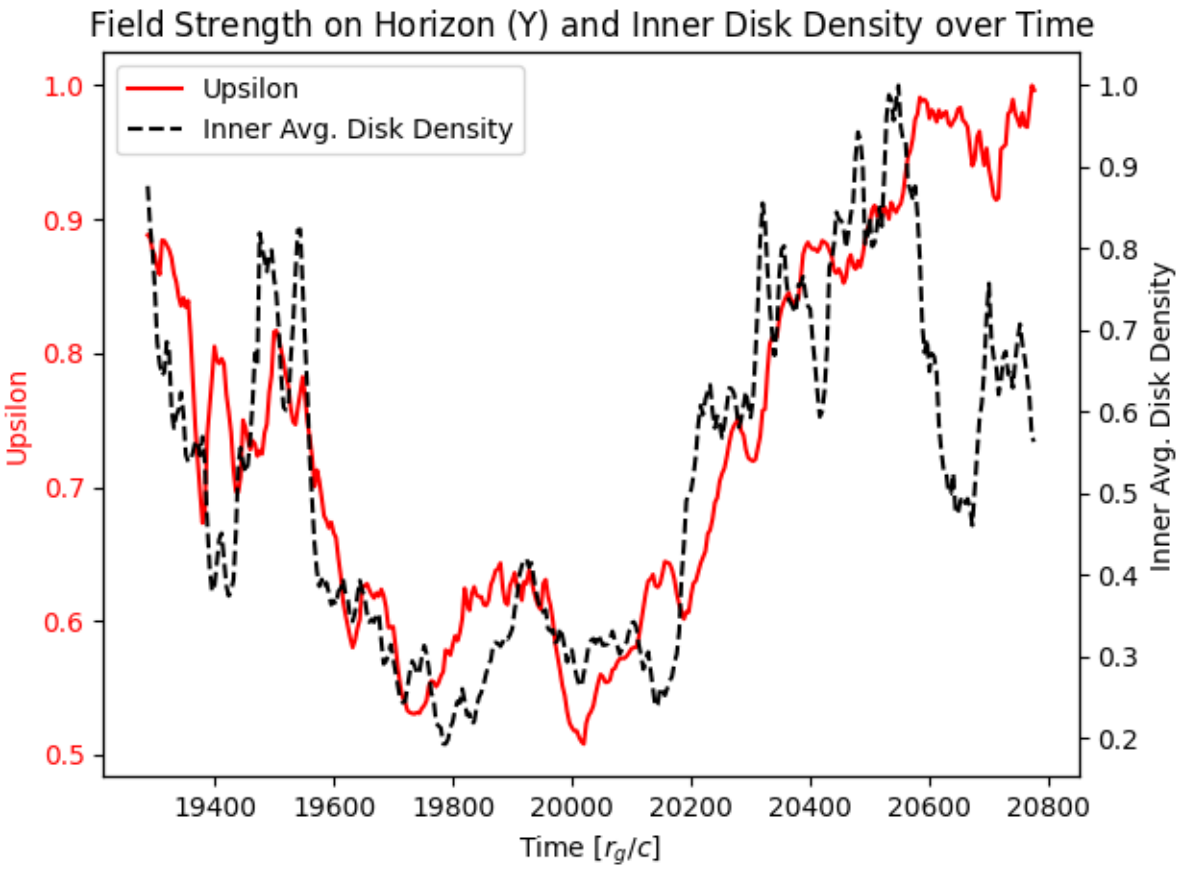

Figure 4.12 Although sharing many common features, average inner annulus density (black, dashed) trails Υ (red, solid), rather than leading Υ.

4.4 A Note on Normalization

Normalizing these new quantities between zero and one, and performing a cross-correlation during the time interval in which Υ's sudden dip occurs, actually did alter the shape of the correlation functions. In some cases, the maximum of this correlation function appeared at a timestep that would suggest a significant time delay. For example, the correlation between Υ and the average gas pressure in the middle annulus had a maximum located $36r_g/c$ from zero, suggesting that the gas pressure in this region may influence the dynamics of Υ during this time interval.

However, the shape of a cross-correlation function is only invariant when scaling the inputs, not shifting them. Thus, normalizing the signals between zero and one should be no different from subtracting off the minimum value of each signal before correlating them. From a brief review of astrophysics literature, I was not able to confirm that this is a standard way to analyze time series in an astrophysical context. For instance, the time-dependent Pearson correlation coefficient, sometimes used in time-series analysis in engineering [Viva Horowitz, private correspondence], is calculated by subtracting the mean of both signals in the cross-correlation, rather than the signal's minimum. However, normalizing the signals in this fashion before performing a cross-correlation does not indicate any significant time-delay.

Ultimately, the significant time delays found when normalizing the functions from zero to one were most likely spurious. While one could argue that normalizing the functions in this way results in a more qualitative interpretation of their cross-correlation, we could not find a precedent for this type of normalization in the context of astrophysical time-series analysis. In addition, these quantities were somewhat naive guesses for the relevant "third" quantity responsible for the sharp dip in both Υ and α during the RT event. As such, it is perhaps not surprising that correlating these quantities with Υ does not suggest an obvious time delay.

Chapter Five

Conclusion

We investigated a simulated RT event in the accretion disk of a spinning, supermassive MAD black hole. Consistent with the findings of Marshall et al. [8], we found that the dominant component of stress was the purely turbulent term, and that outward angular momentum transport decreases, during the RT event. Motivated by the qualitative similarities between Υ and α, we explored the possibility of a causal relationship between the quantities. In search of a lurking explanatory variable, I investigated the average gas pressure and average density in three annuli in the simulated system, but was not able to find significant evidence that any of these quantities influence BH accretion.

This study analyzed only one RT event, though the simulation contains tens of such events. Several of these have been studied as part of similar student theses, and our findings are consistent with their results. This suggests that the observed accretion in black hole accretion disks may be due to a different type of instability altogether, such as the Kelvin-Helmholtz instability. However, the remainder of these RT events ought to be studied in our simulation before making such a conclusion.

REFERENCES

[1] Albert Einstein. "Die Feldgleichungen der Gravitation". In: *Sitzungsberichte der Königlich Preußischen Akademie der Wissenschaften (Berlin)* (Jan. 1915), pp. 844–847.

[2] Karl Schwarzschild. "Über das Gravitationsfeld eines Massenpunktes nach der Einsteinschen Theorie". In: *Sitzungsberichte der Königlich Preußischen Akademie der Wissenschaften (Berlin)* (Jan. 1916), pp. 189–196.

[3] Kip S. Thorne. *Black holes and time warps : Einstein's outrageous legacy*. eng. 1st ed. The Commonwealth Fund Book Program. New York: W.W. Norton, 1994. ISBN: 0393035050.

[4] Event Horizon Telescope Collaboration, Kazunori Akiyama, Antxon Alberdi, et al. "First M87 Event Horizon Telescope Results. I. The Shadow of the Supermassive Black Hole". In: 875.1, L1 (Apr. 2019), p. L1. DOI: 10.3847/2041-8213/ab0ec7. arXiv: 1906.11238 [astro-ph.GA].

[5] Mitchell C. Begelman. "Accreting Black Holes". In: *arXiv e-prints*, arXiv:1410.8132 (Oct. 2014), arXiv:1410.8132. arXiv: 1410.8132 [astro-ph.HE].

[6] James M. Stone and Thomas Gardiner. "The Magnetic Rayleigh-Taylor Instability in Three Dimensions". In: 671.2 (Dec. 2007), pp. 1726–1735. DOI: 10.1086/523099. arXiv: 0709.0452 [astro-ph].

[7] Mark J. Avara, Jonathan C. McKinney, and Christopher S. Reynolds. "Efficiency of thin magnetically arrested discs around black holes". In: 462.1 (Oct. 2016), pp. 636–648. DOI: 10.1093/mnras/stw1643. arXiv: 1508.05323 [astro-ph.HE].

[8] Megan D. Marshall, Mark J. Avara, and Jonathan C. McKinney. "Angular momentum transport in thin magnetically arrested discs". In: 478.2 (Aug. 2018), pp. 1837–1843. DOI: 10.1093/mnras/sty1184. arXiv: 1709.10113 [astro-ph.HE].

[9] Charles W. Misner, Kip S. Thorne, and John Archibald Wheeler. *Gravitation / Charles W. Misner, Kip S. Thorne, John Archibald Wheeler*. English. W. H. Freeman San Francisco, 1973, xxvi, 1279 p. : ISBN: 0716703343 0716703440.

[10] E. T. Newman, E. Couch, K. Chinnapared, et al. "Metric of a Rotating, Charged Mass". In: *Journal of Mathematical Physics* 6.6 (June 1965), pp. 918–919. DOI: 10.1063/1.1704351.

[11] J. A. Wheeler and K. W. Ford. *Geons, Black Holes, and Quantum Foam: A Life in Physics*. Miscellaneous. 1998.

[12] James B. Hartle. *Gravity : an introduction to Einstein's general relativity*. 2003.

[13] Steven A. Balbus and John F. Hawley. "Instability, turbulence, and enhanced transport in accretion disks". In: *Rev. Mod. Phys.* 70 (1 Jan. 1998), pp. 1–53. DOI: 10.1103/RevModPhys.70.1. URL: https://link.aps.org/doi/10.1103/RevModPhys.70.1.

[14] Derek Hung, Eric Blackman, Kyle Caspary, et al. "Experimental confirmation of the standard magnetorotational instability mechanism with a spring-mass analogue". In: *Communications Physics* 2 (Jan. 2019). DOI: 10.1038/s42005-018-0103-7.

[15] Feng Yuan and Ramesh Narayan. "Hot Accretion Flows Around Black Holes". In: 52 (Aug. 2014), pp. 529–588. DOI: 10.1146/annurev-astro-082812-141003. arXiv: 1401.0586 [astro-ph.HE].

[16] N. I. Shakura and R. A. Sunyaev. "Black holes in binary systems. Observational appearance." In: 24 (Jan. 1973), pp. 337–355.

[17] Karina Sirabian. "Examining the Effects of the Magnetic Rayleigh-Taylor Instability in Thin Magnetically-Arrested Accretion Disks Around Black Holes". Hamilton College, 2020.

[18] Calen Carron. "Magnetic Rayleigh-Taylor Bubble Disruptions and Their Effect on the Magnetic Field in a Black Hole Accretion Disk Simulation". Hamilton College, 2020.

[19] Qianqian (Jade) Xu. "Outward Transportation of AngularMomentum [sic] in Magnetic Rayleigh-Taylor Instability Model and its Relationship with Accretion of Black Holes". Hamilton College, 2020.

[20] H. Alfvén. "Existence of Electromagnetic-Hydrodynamic Waves". In: 150.3805 (Oct. 1942), pp. 405–406. DOI: 10.1038/150405d0.